Impact of the redox state of flavin chromophores on the UV–vis spectra, redox and acidity constants and electron affinities

Padmabati Mondal, Karno Schwinn, Miquel Huix-Rotllant

Impact of the redox state of flavin chromophores on the UV–visible spectra, redox and acidity constants and electron affinities

Padmabati Mondal*, Karno Schwinn, Miquel Huix-Rotllant**

Aix Marseille Univ, CNRS, ICR, Marseille, France

Abstract

Isoalloxazine is the core chromophore present in the cofactor of flavoproteins. Naturally, flavin usually exists in five different redox forms in protein milieu by accepting up to 2-electrons and 2-protons. The redox state has a strong impact on its photophysical properties. Fully oxidized and anionic radical isoalloxazine absorb blue light, neutral semi-quinone form absorbs green/red light and fully reduced forms absorb UV light. In the excited state, isoalloxazine becomes a strong oxidizer and acidic upon reduction. Understanding the relation between the redox form and its photophysical properties is fundamental to understand the biochemistry of flavoproteins. Here, we compare the effect of the redox state of isoalloxazine and some derivates on the UV-visible spectra, the redox potentials, acidity constants and electron affinities by means of electronic structure simulations. We show that the physical properties are directly related to a transformation of a α-diimine bond to a ethene-1,2-diamine bond upon reduction.

Keywords: flavins, vibrationally resolved spectra, redox potentials, acidity constants, electron affinities

1. Introduction

Flavoproteins are involved in numerous cell functions ranging from bioluminescence [1], redox reactions [2, 3], DNA repair, [4, 5], magnetoreception, [6, 7] photosynthesis, [8] cell apoptosis, [9, 10], detoxification, [11, 12], blue-light sensors like phototropins, [13, 14] etc. Most flavoproteins have a vitamin B_2 cofactor (riboflavin) either in the form of flavin mononucleotide or flavin adenine dinucleotide. Isoalloxazine is the main chromophore in all flavin derivatives. Isoalloxazine is a well known photo-oxidizing agent. [15, 16] In its fully oxidized form, it can accept up to two electrons. The anionic reduced species are acidic and a proton transfer can follow after each electron transfer. [17] Therefore, in the present study we focus on five different redox states (see Fig. 1): the fully oxidized isoalloxazine (FLA), two semi-quinone forms (anionic, $FLA^{\bullet-}$ and neutral, $FLAH^{\bullet}$) and two reduced hydroquinones (anionic, $FLAH^-$ and neutral, $FLAH_2$).

The rich photophysics and photochemistry of isoalloxazine and related derivates have been of much interest both experimentally [18, 19, 20, 21, 22, 23, 24, 25] and theoretically. [26, 27, 28, 29, 30, 31, 32, 33, 34, 35] From a theoretical point of view, the simulation of the UV-visible spectrum is very challenging. The fully oxidized isoalloxazine form is perhaps the best studied theoretical

model, despite being an unstable tautomer in solution.[25] Two broad absorption bands are found at 440-450 nm in the blue light region and a near-UV band at 333 nm respectively, [18, 25] corresponding to a $\pi \rightarrow \pi^*$ transition. These bands are characteristic absorption peaks of flavins found in flavoproteins.[36, 37, 38] The origin of this absorption has been difficult to attribute theoretically.[39, 40] Most common electronic structure methods predict a blue-shifted absorption maximum when applying the Franck-Condon principle (clamped nuclei approximation). Time-dependent density-functional theory (TD-DFT) with the popular B3LYP functional leads to a lowest bright state absorption maximum of 408 nm for lumiflavin [24, 41]. Serrano-Andrès *et al.* applied multi-configuration perturbation theory to isoalloxazine, obtaining 401 nm absorption maximum, similar to the 407 nm obtained with QM/MM multi-configuration simulations for flavin adenine dinucleotide embedded in plant cryptochrome. [42] Multi-reference DFT CI of Grimme and coworkers lead to a 422 nm absorption maximum for lumiflavin, [32] closer to the experimental value. Second-order perturbation theory Green's function approach lead to the same absorption peak.[43]

The absorption bands of flavins have a strong vibrational structure, which has to be taken into account in the simulation of the spectrum. On the one hand, classical molecular dynamics have been used to include inhomogeneous broadening.[40] This is especially important for riboflavin, in order to take into account hydrogen bond interactions and also the interaction with the solvent.[44] On the other hand, the homogeneous broadening due to the internal isoalloxazine vibrations is fundamental to re-

---

*Corresponding author

**Corresponding author

Email addresses: padmabati.mondal@univ-amu.fr (Padmabati Mondal), miquel.huixrotllant@univ-amu.fr (Miquel Huix-Rotllant)
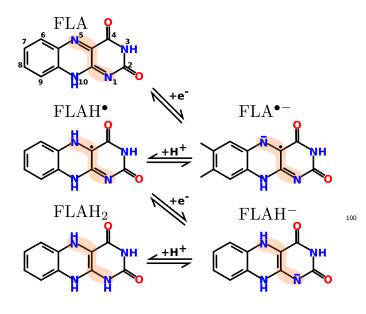
Figure 1: Lewis structures of isoalloxazine (FLA) and radical anion (FLA$^{\bullet-}$), neutral radical (FLAH$^{\bullet}$), reduced anionic (FLAH^{-}) and reduced neutral (FLAH$_2$) forms. The redox and acid-base reactions that connect each structure are shown. The whole reactivity happens between atoms $N_1=C_{10a}$-$C_{4a}=N_5$, highlighted as a orange-shaded area. Atom numbering is shown on FLA.

produce the three-peak structure of the lowest absorption band [34, 45] Saalfrank *et al.* showed that C-N stretchings around 1600 cm^{-1} are responsible of the large broadening of the lowest absorption band in a range of about 50 nm.[34] Indeed, the 408 nm absorption of riboflavin with TD-DFT in the Franck-Condon approximation leads to a three bands when vibrations are taken into account, with maxima at 448, 425 and 404 nm, closely resembling the experimental bands 468, 443 and 415 nm.[34] Very recently, Solov'yov et. al. simulated the absorption spectrum of lumiflavin in different redox states embedded in protein using QM/MM approach, obtaining a good agreement with the experimental absorption spectra. [46]

FLA fluorescent emission has been well studied experimentally, but it is currently attracting much attention as it can be very selectively detected in biological medium. Flavin-based fluorescent proteins can be used for imaging. [47] There are few theoretical studies which have focused on the simulation of emission of flavins. [48, 49, 50] The fluorescent emission spectrum shows a broad band around 550 nm. [51] This maximum is very much affected by the interactions with the protein residues. [50] These spectroscopic properties of FLA depend strongly on the pH. [51] Indeed, the atoms N_1, N_3 and N_5 are acidic centers, the pK$_a$ of which depends on the redox state. [51, 29]

Most of the previous studies have focused on the photophysics of the fully oxidized FLA. Recently, a systematic comparison of steady state and time-resolved absorption and fluorescence spectra of five different redox states of flavin in solution and in protein milieu have been investigated experimentally. [17] In this study, it was found that

fully oxidized and anionic radical isoalloxazine absorb blue light (445-450 nm), partially reduced neutral form absorb green/red light (500-600 nm) and fully reduced forms absorb UV light (350-375 nm). Ultrafast excited state decay of flavin radical species was observed with a rapid access to the conical intersection via a bending motion of the isoalloxazine ring. This fast internal conversion occurs in solution but not in the protein due to a restricted access to the conical intersection.

A systematic theoretical study of the electronic structure of different redox states and their photophysical properties is fundamental to understand the functioning of flavoproteins. Here, we describe the effect of the redox state on the absorption and emission spectra, redox potential, acidity constants, as well as on the electron affinities by means of density functional theory (DFT) and its time-dependent extension. Indeed, we relate the difference in the electronic density distributions among the rings conforming isoalloxazine for different redox states to their photophysical properties. We show that the physical properties are directly related to a transformation of a α-diimine bond to a ethene-1,2-diamine bond upon reduction, by populating a π-type orbital which is bonding for the C-C single bond and antibonding for the N=C double bonds of the diimine group.

2. Computational details

Vibrationally resolved spectra. The vibrationally resolved absorption and emission spectra for the five molecules have been calculated using the time-dependent path integral method from the Fourier transform of the time-dependent autocorrelation function, as implemented in GAUSSIAN 16. [52] These computations require the minimum energy structures of both the ground and excited states and the frequencies at each minimum. The excited state frequency and normal modes were obtained using the (TD-)DFT in conjunction with the B3LYP exchange correlation functional. [53, 54] For these calculations, we employed the def2-TZVPP basis set. This functional was recently successfully applied and showed best performance for the calculation of the vibronic absorption and emission spectrum of lumiflavin derivatives. [45] All vibrationally resolved spectra simulations have been performed in ethanol using a polarizable continuum model (PCM) scheme. [55, 56] For the path-integral approach, 2^{20} integration steps were used and for the convolution of the spectrum, homogeneous and inhomogeneous broadening of 235 cm^{-1} were employed. All modes of the isoalloxazine ring were considered for the calculation of the spectrum. Whenever possible, we have also applied the sum-over state approach to analyze the origin of the peaks. [57]

Photoredox potentials and pK$_a$s. For the calculation of (photo)redox potential of different reduction processes involving flavin, the Gibbs free energy (G) were obtained from the theormochemistry calculations using (TD-)DFT

at the B3LYP/def2-TZVPP level in the ground and excited states of different redox states of flavin in the gas phase and in ethanol (using PCM). The change is Gibbs free energy ($\Delta G_\mathrm{S}^\mathrm{rdx}$) for a process in solution was then calculated using the Born-Haber Cycle.

$$\Delta G_\mathrm{S}^\mathrm{rdx} = \Delta G_\mathrm{S}^\mathrm{0,red} + \Delta G_\mathrm{S}^\mathrm{ox} - \Delta G_\mathrm{gas}^\mathrm{rdx} \qquad (1)$$

Using the Nernst equation, the relation between the $\Delta G_\mathrm{S}^\mathrm{rdx}$ (eV) and the reduction potential, E^0 (V) for a one electron redox reaction is given as

$$E^0 = -\Delta G_\mathrm{S}^\mathrm{rdx} \qquad (2)$$

Finally, the absolute reduction potential of ferrocene electrode is substracted from the E^0 resulting in E_{calc}^0 which can be directly compared to the available experimental redox potentials. The absolute reduction potential of ferrocene electrode in DMSO (4.89 V) is taken from Ref. 58.

The pK_a value for a deprotonated species is calculated from the thermodynamic cycle of a protonation reaction. The pK_a value for a single molecule was calculated using the following equation

$$pK_a = \frac{\Delta G_\mathrm{aq}}{k_b T ln(10)} \qquad (3)$$

where

$$
\begin{aligned}
\Delta G_\mathrm{aq} &= \Delta G_\mathrm{gas} + \Delta\Delta G_\mathrm{S} \qquad (4)\\
\Delta G_\mathrm{gas} &= G_\mathrm{gas}(H^+) + G_\mathrm{gas}(A^-) - G_\mathrm{gas}(HA)\\
\Delta\Delta G_\mathrm{S} &= \Delta G_\mathrm{S}(H^+) + \Delta G_\mathrm{S}(A^-) - \Delta G_\mathrm{S}(HA).
\end{aligned}
$$

where the values of $\Delta G_\mathrm{gas}(H^+)$ and $\Delta G_\mathrm{S}(H^+)$, -0.27 eV and -11.56 eV, respectively, are taken from Ref. 59 and Ref. 60. The higher pK_a value of the deprotonated species correspond to higher proton affinity i.e. lower acidity of the protonated species and vice versa.

Electron affinities. First electron affinities corresponding to the process $A + e^- \rightarrow A^-$ have been obtained from the equation

$$EA = E(X) - E(X^-) \qquad (5)$$

in which $E(X)$ and $E(X^-)$ correspond to the total electronic energies at the minimum energy structure of the neutral molecule and the anionic molecule respectively. The optimizations have been performed at the B3LYP/def2-TZVPP level of theory, and the energies to compute the electron affinities have been computed at the B3LYP/aug-cc-pVQZ+2df level. All calculations have been performed in GAUSSIAN16. [61]

3. Results and Discussion

The reduction of flavin has a strong impact in the photophysical properties of isoalloxazine moiety. In order to understand the effect of the redox state on isoalloxazine, it is important to discuss first the main electronic and structural changes that occur during the redox and acid-base reactions. The electronic density is mostly affected on the atoms forming the α-diimine bond, found between atoms $N_1=C_{10a}-C_{4a}=N_5$ (see shaded area in Fig. 1).

The fully oxidized isoalloxazine is planar, even though it is not a completely delocalized aromatic system. The first reduction leads to the anionic semi-quinone FLA$^{\bullet-}$. In the simplest Lewis structure, the radical electron sits on C_{4a} and a negative charge is located on N_5. However, the planarity of this molecule induces a delocalization of the electronic and spin densities over the three rings. FLA$^{\bullet-}$ is acidic, and a subsequent proton transfer reaction can occur that stabilizes the negative charge, forming the neutral semi-quinone FLAH$^\bullet$. The ground state of FLAH$^\bullet$ is planar also, despite the apparent secondary amine structure that is formed in N_5. This is because of the delocalized spin density mainly between the C_{4a} and N_5 center. A subsequent reduction of FLAH$^\bullet$ forms the anionic hydroquinone FLAH$^-$, which is non-planar ("butterfly") in its ground state. The $N_1=C_{10a}-C_{4a}=N_5$ bond becomes rather a ethene-1,2-diamine, in which N_1 allocates the negative charge. The anionic hydroquinone can accept an extra proton producing the fully reduced hydroquinone FLAH$_2$, which is non-planar due to the presence of two secondary amines in N_5 and N_1.

The five isoalloxazine forms have clearly distinct electronic structure. Figure 2 shows the Walsh diagram of molecular π-orbitals along with the simplified depiction of the orbital density of each form of FLA. For all redox forms, molecular orbitals are similar in shape. Most molecular orbitals are typical π-type orbitals, delocalized over the phenyl or uracyl rings. However, orbital π_3 has special characteristics. This orbital is anti-bonding between the $N_5=C_{4a}$ (imine bond) centers and bonding between $C_{4a}-C_{1a}$ (ethylene bond). This orbital receives electrons when FLA is reduced, thus explaining why the double-bond pattern changes. It is the lowest unoccupied molecular orbital (LUMO) of FLA, the single occupied molecular orbital (SOMO) for radical semi-quinones and the highest occupied molecular orbital (HOMO) for reduced forms. The different occupations of this orbital affects the photophysical properties of each redox form.

3.1. Absorption and emission spectra

The electronic absorption spectra in the Franck-Condon approximation for the five redox states at the TD-B3LYP level and the def2-TZVPP basis set are shown in Tab. 1.

The oxidized form is the better studied form of isoalloxazine. The lowest bright state corresponds to a HOMO→LUMO transition. The HOMO is a π orbital delocalized over the whole structure but with a large contribution of the phenyl

Table 1: Electronic absorption spectrum in the Franck-Condon approximation for the 5 redox species derived from FLA. The analysis of the transitions is given along with the wavelength (in nm) and the oscillator strength (in arbitrary units). The "n" orbital generically stands for a lone pair electron in oxygen, while the "π" orbitals are specified in Figure 2. Experimental results for FLA are taken from Ref. 25, for FLA$^{\bullet-}$ and FLAH$^\bullet$ are taken from Ref. 62, while FLAH$^\bullet$ and FLAH$_2$ have been taken from Ref. 63.

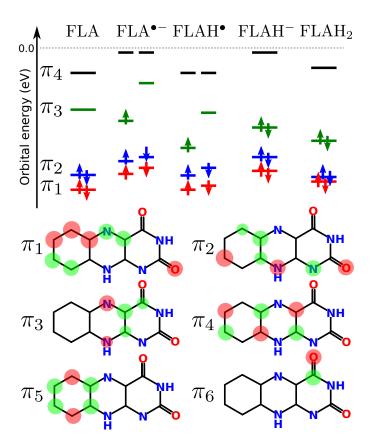|	Transition	Excit.	f	Exp.
FLA	$\pi_2 \to \pi_3$	391	0.247	410
	n$\to \pi_3$	367	0.002	
	n$\to \pi_3$	349	0.000	
	$\pi_1 \to \pi_3$	326	0.260	
FLA$^{\bullet-}$	$\pi_3^\alpha \to \pi_4^\alpha$	535	0.004	
	$\pi_3^\alpha \to \pi_5^\alpha$	437	0.002	
	$\pi_2^\beta \to \pi_3^\beta$	423	0.130	485
	n$^\beta \to \pi_3^\beta$	391	0.001	
	$\pi_1^\beta \to \pi_3^\beta$	359	0.101	367
	$\pi_3^\alpha \to \pi_6^\alpha$	337	0.291	
	n$^\beta \to \pi_3^\beta$	335	0.000	
FLAH$^\bullet$	$\pi_2^\beta \to \pi_3^\beta$	535	0.132	571
	$\pi_3^\alpha \to \pi_4^\alpha$	428	0.019	
	$\pi_1^\beta \to \pi_3^\beta$	406	0.059	485
	n$^\beta \to \pi_3^\beta$	405	0.000	
	$\pi_3^\alpha \to \pi_5^\alpha$	351	0.076	
	n$^\beta \to \pi_3^\beta$	348	0.029	
	n$^\beta \to \pi_3^\beta$	341	0.000	
	n$^\beta \to \pi_3^\beta$	331	0.000	
	$\pi_0^\beta \to \pi_3^\beta$	296	0.113	340
FLAH$^-$	$\pi_3 \to \pi_4$	386	0.006	
	$\pi_3 \to \pi_5$	347	0.121	342
	$\pi_3 \to \pi_6$	271	0.280	285
FLAH$_2$	$\pi_3 \to \pi_4$	400	0.025	395
	$\pi_3 \to \pi_5$	319	0.116	
	$\pi_3 \to \pi_6$	287	0.221	295

Figure 2: (top) Walsh-like diagram of molecular orbitals for the different redox states of isoalloxazine ring. The alpha and beta orbitals are shown for radicals. (bottom) Schematic representation of the π orbitals (green and red filled circles represent positive and negative lobes).

ring, while the LUMO is a π^* that debilitates the N$_5$=C$_{4a}$ double bond. This transition is located at 391 nm, closely reproducing the experimental maximum, predicted at 410 nm.[25] The second bright state corresponds to a HOMO-1$\to$LUMO transition of a similar oscillator strength as the first state, found at 326 nm. In between these two peaks, two dark transitions are found corresponding to the oxygen lone pair to the π_3^* orbital.

For the radical anion FLA$^{\bullet-}$, equivalent bright transitions to FLA are found at 423 nm and 337 nm, involving $\pi_2 \to \pi_3^*$ and $\pi_1 \to \pi_3^*$ transitions respectively. These transitions are red-shifted compared to FLA due to the presence of an extra electron. Indeed, two almost dark transitions involving the radical are found below in energy to the first bright transition, involving transitions from π_3 which is now partially occupied. The first bright transition is predicted about 60 nm blue-shifted with respect to experiments, while the second bright peak closely matches the experimental value.

The neutral radical FLAH$^\bullet$ has a noticeably different absorption spectrum. Theory predicts its first bright state at 535 nm, 40 nm blue-shifted with respect to experiments. It corresponds to a $\pi_2 \to \pi_3$ transition. The equivalent
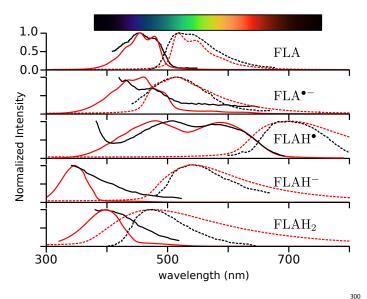
Figure 3: Comparison of the experimental (black) and theoretical (red) absorption (solid) and emission spectra (dashed) for the five redox forms of isoalloxazine. For the sake of comparison, theoretical spectrum maxima have been shifted to the experimental values. Experimental data has been taken from Refs. 17, 64 and 63. Experimental absorption and emission spectra of FLA are taken from the flavin mononucleotide spectra in flavodoxin, [17] as well as emission of FLAH$^-$ from flavin mononucleotide in flavodoxin. [64] Experimental absorption spectrum for FLAH$^-$ and FLAH$_2$ are taken from flavin mononucleotide spectra in water solution. [63]. The spectra of FLA$^{\bullet-}$ is taken from cryptochrome flavin adeninde dinucleotide [17], FLAH$_2$ emission from flavin adenine dinucleotide in solution [17] and FLAH$^\bullet$ absorption spectrum is taken from absorption spectra of methylated flavin radical [65] and emission spectrum is taken from flavin mononucleotide in flavodoxin. [64] The visible spectrum range is shown as an offset.

transition for the radical anion is found 100 nm higher in energy. Indeed, the relaxation induced by the neutralization of the negative charge by the H$^+$ has a strong impact in the absorption spectrum. The second bright state, found at 406 nm, is 85 nm above the experimental value, and it corresponds to a $\pi_1 \rightarrow \pi_3$ transition. Finally, the highest bright state is found at 296 nm, about 35 nm above the experiments.

The fully reduced anion (FLAH$^-$) and neutral (FLAH$_2$) forms have very similar absorption spectra. Unlike the oxidized and semi-quinonic forms, the transitions of the reduced flavins do not involve transitions to π_3 orbital, which are responsible for the lowest bright absorption bands. Indeed, the first bright transition for FLAH$^-$ is predicted at 347 nm, similar to the experimental value of 342 nm, involving a transition of the type $\pi_3 \rightarrow \pi_5$. The second bright state is predicted at 271 nm (for an experimental value of 285 nm) is interpreted as a $\pi_3 \rightarrow \pi_6$.

For the FLAH$_2$ form a similar trend is observed as for FLAH$^-$. The first bright state is found at 319 nm, while the second bright state is found at 287 nm (for an experimental value of 295 nm). They are interpreted as $\pi_3 \rightarrow \pi_5$ and $\pi_3 \rightarrow \pi_6$ respectively.

Vibrationally resolved spectra. The theoretically predicted absorption maximum in the Franck-Condon approximation does not correctly reproduce the color of absorption, especially for FLA, FLA$^{\bullet-}$ and FLAH$^\bullet$. Both FLA and FLA$^{\bullet-}$ absorb blue light and emit green light. FLAH$^\bullet$ has a broad absorption band in the green region and emits in the dark red region. Finally, FLAH$^-$ and FLAH$_2$ absorb in the UV region and emit green light.

In order to reproduce the broadening of the spectra, explicit account of vibrations has to be taken into account in the simulation of the spectrum. Indeed, the absorption spectra of isoalloxazine and related derivates have a broad and pronounced vibrational structure for each of the electronic transitions. In Fig. 3, we show the simulated vibrationally resolved absorption and emission spectra in the visible light region. The vibrationally resolved theoretical absorption and emission spectra are shown in comparison to the experimental spectra. [17, 64, 63, 65] For the radical semi-quinones (FLA$^{\bullet-}$ and FLAH$^\bullet$), we compare to the absorption spectra of FAD$^{\bullet-}$ in cryptochrome [17] and of 5CH$_3$FMN$^\bullet$ in D$_2$O[65] respectively, which are similar to the absorption spectra in solution. [66] For the sake of comparison, we apply a shift of the 0-0 transition for absorption and emission to match the experimental peak maxima (see Supporting Information for details).

The absorption spectrum of the oxidized form of FLA shows a four-peak vibrational structure, found at 451, 447, 443 and 439 nm, with dipole strength of 0.295, 0.383, 0.245 and 0.103 respectively, corresponding to the $\pi_2 \rightarrow \pi_3$ electronic transition. The first peak arise from the 0→0 transition, and the three other peaks correspond to the 0→5^1, 0→5^2 and 0→5^3 vibrational transitions of the in-plane symmetric bending of the uracil and phenyl rings with respect to the center ring. The emission spectrum of FLA, corresponding to the $\pi_2 \leftarrow \pi_3$ transition, a three peak structure is observed at 460 nm, 480 nm and 550 nm. The first peak is represented as a combination of 0→0 transition and the 0→5^1, 0→5^2 and 0→5^3 transitions. The second and third peak correspond respectively to double vibrational excitations of the type 0→5^{1}38^1 and 0→5^{1}50^1, in which vibration 38 is a combination of N$_3$-C$_4$ and N$_1$-C$_2$ stretching modes, and vibration 50 is a combination of N$_5$-C$_{4a}$ and N$_{10}$-C$_{10a}$ stretching modes.

The spectrum of FLA$^{\bullet-}$ shows an analogous trend to that of the FLA. The $\pi_2 \rightarrow \pi_3$ transition of the anionic radical is in the similar region of that of FLA, in addition to an almost dark $\pi_3^\alpha \rightarrow \pi_4^\alpha$ transition between 500-600 nm involving the SOMO electron. The $\pi_2 \rightarrow \pi_3$ transition has a similar vibrational progression to FLA, involving single vibrational transitions of in-plane bending in addition to other in-plane stretching modes involving vibration 38 (N$_3$-C$_4$ and N$_1$-C$_2$ stretching modes), and vibration 50 (N$_5$-C$_{4a}$ and N$_{10}$-C$_{10a}$ stretching modes). The dark $\pi_3^\alpha \rightarrow \pi_4^\alpha$ transition is represented by out-of-plane motions delocalized over the whole structure, N$_3$-H hydrogen out-of-plane motion and C$_{6a}$-C$_{9a}$ stretching and N$_{10}$-C$_{10a}$ stretching.

5

For FLAH$^\bullet$, FLAH$^-$ and FLAH$_2$, the peaks does not show a clear vibrational progression, probably due to the larger contribution of low-frequency out-of-plane modes. Indeed, either the ground- or the excited state minimum energy structure is in a "butterfly" conformation. The vibrationally resolved theoretical spectra for FLAH$^\bullet$ is in good agreement with experiments, showing a two broad double absorption peaks at ca. 600 nm and 500 nm, and a single emission peak at 700 nm.

Only a moderate agreement is observed between theoretical and experimental absorption spectra for the forms FLAH$^-$ and FLAH$_2$. The theoretical absorption spectra shows a sharp peak for both species, while the experimental peak shows a broader band. This disagreement might be due to three reasons: (i) reduced forms of riboflavin tend to aggregate in solution [67], (ii) a keto-enol equilibrium of fully reduced isoalloxazine between N$_1$H-C$_2$=O and N$_1$=C$_2$-OH forms, and (iii) an overlap of the vibrational structure of higher-energy states that we did not consider in our simulation.

For the emission of FLAH$^-$ and FLAH$_2$, a reasonable agreement is observed. For FLAH$^-$, the experimental emission spectrum maximum is around 450 nm for a W60F/Y98F flavodoxin mutant.[68] The wavelength of this emission is very much dependent on the protein environment, and in the literature this emission has been reported at 530 nm for the wild-type protein, similar to FADH$_2$.[69] Theoretical studies have shown that the protein-flavin interactions and the hydrogen-bond network are fundamental to describe this wavelength.[50] This is however beyond the scope of the present theoretical study.

Effect of substitutions. Isoalloxazine is an unstable molecule in solution.[25] More stable forms of isoalloxazine are frequently found, in which positions C$_7$ and C$_8$ are methylated, the so-called 7,8-dimethylisoalloxazine or lumichrome. In addition, R-substitutions on N$_{10}$ are frequently found to form lumiflavin (R=CH$_3$) or riboflavin (R=ribitol). In Fig. 4 we show the effect of these substitutions on the vibrationally resolved absorption spectra for the fully oxidized form in ethanol compared to experimental values. Overall, we can observe a good match between the vibrational structure of the theoretical and experimental spectra. We observe that the methylation of positions 7 and 8 induces a red-shift of the absorption maxima.[25] The origin of this red shift is probably due to the sigma bond resonance effect (hyperconjugation) which induces a bathochromic shift in conjugated systems.[70] Hydrogen bonding with the solvent or the ribitol in the case of riboflavin can further explain the red-shift of the main peaks. Irrespective of the form, we observe the typical vibrational progression for the two well-separated electronic transitions corresponding to $\pi_2 \to \pi_3^*$ and $\pi_1 \to \pi_3^*$ transitions respectively. Interestingly, the latter peak is formed by the contribution of three electronic transitions, mainly $\pi_1 \to \pi_3^*$, with minor contributions from transitions from lower π orbitals.

3.2. Redox potentials and acidity constants

The redox and acidity properties of flavin derivatives have been a matter of intense study in the literature. [71, 72, 73, 74, 58, 75] Here, we compare the computed reduction and photo-reduction potentials (E^0_{calc}) and acidity constants (pK$_{a,calc}$) for the main flavins' redox and acid-base reactions depicted in Fig. 1. Usually, the reported redox values in the literature correspond to the one electron/one proton or two electron/two proton processes. Here, we compare the redox processes against individual reactions obtained for riboflavin in dimethyl sulfoxide. [71, 58]

The (photo)redox potentials are reported in Table 2. Here, we use a ferrocene electrode as reference. The comparison of calculated reduction potential with other experimental values with reference to standard hydrogen electrode (absolute reduction potential = 4.24 V [76]) is given in the Supporting Information. We recall the convention $E^0_{calc} > 0$ for oxidizing agent, while $E^0_{calc} < 0$ for reducing agents. We first discuss the results for isoalloxazine. Both oxidized form of FLA and the neutral semiquinone FLAH$^\bullet$ are weakly reducing agent in their ground states. The reduction potentials of FLA is -1.16 V, in line with the experimental oxidation -1.21 V for 10-isopropyl-isoalloxazine. The reduction potential for FLAH$^\bullet$ -1.07 V, smaller than FLA. Flavins become a strong oxidizing agent when excited. [77] Indeed, we find that both FLA and FLAH$^\bullet$ become strong oxidizing agents in the excited state with a photoredox potential of +1.57 V and +1.1 V for FLA and FLAH$^\bullet$ respectively. Oxidized flavins undergo intersystem crossing upon photon absorption, leading to a certain amount of triplet state flavin. [78] The photoredox potential from the triplet FLA gives +0.80 V, a moderately high oxidizing agent but less strong than in the singlet state. This effect is expected, due to the fact that triplet states in neutral organic molecules are usually more energetically stable than the singlet states. We have also considered competing reduction reactions when the N$_1$ acidic site is protonated instead of N$_5$ for the anionic semi-quinone (FLAH'$^\bullet$). In this case, the ground state reduction potential becomes -1.79 V, being thus a much stronger reducing agent than FLAH$^\bullet$ when N$_5$ is protonated. When excited, FLAH'$^{*\bullet}$ becomes a much weaker oxidizing agent (0.03 V) than FLA* and FLAH$^{*\bullet}$.

The variance of reduction potentials in the ground state and excited state can be related to the change in electron affinities (Fig. 2). Indeed, in the ground state of FLA, an electron has to be injected in the π_3 orbital to be reduced to FLA$^{\bullet-}$. The electron affinity (estimated from the energy of the LUMO orbital) is -0.14 eV. Upon FLA excitation, a $\pi_2 \to \pi_3$ transition occurs. If the excited state is sufficiently long-lived, the electron will be injected in the π_2 orbital upon reduction of excited FLA. The electron affinity of π_2 orbital is about -0.24 eV, which explains the stronger oxidizing capacity of FLA in the excited state. A very similar trend is observed for the case of FLAH$^\bullet$ →FLAH$^-$ reaction. For the neutral semi-quinone
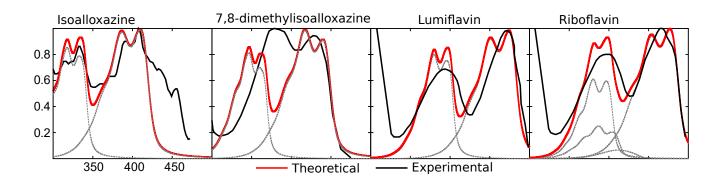
Figure 4: Comparison of experimental (black) and theoretical (red) absorption spectrum for isoalloxazine, 7,8-dimethylisoalloxazine, lumiflavin and riboflavin in ethanol. The theoretical spectrum in red corresponds to the total spectrum of all excited states, while the grey dotted line shows the contribution of a single state. All spectra has been normalized to the highest intensity peak in the range between 300 nm and 500 nm. The spectra of isoalloxazine, lumiflavin and riboflavin have been shifted 10, 35 and 35 nm respectively to match the experimental spectral maximum. The experimental spectra for isoalloxazine (in water) has been taken from Ref. 25. The other experimental spectra were recorded in ethanol. The 7,8-dimethylisoalloxazine was taken from Ref. 20 and lumiflavin and riboflavin from Ref. 19.

in the ground state, the electron has to be injected in the π_3 orbital, which leads to an estimate of the electron affinity of -0.13 eV. Upon excitation, a $\pi_2 \rightarrow \pi_3$ transition occurs. Thus, similar to the case of FLA, the π_2 orbital becomes vacant, leading to an electron affinity of -0.23 eV. The small differences that are observed in the E_{calc}^0 for FLA and FLAH$^\bullet$ can be attributed to both the difference in ΔG_{gas}^{redox} and the solvation effect (see Supporting Information).

The effect of 7,8-dimethyl substitutions and N_{10} substitutions on the redox potentials has been also a matter of intense discussions in the literature. [79, 80, 72, 81] In general, it has been concluded that the effect of methyl substituents in the flavin ring has only a minor effect. The redox potential for 7,8-dimethylisoalloxazine, lumiflavin and riboflavin are -1.29 V, -1.35 V and 1.33 V respectively, close to the -1.16 V of isoalloxazine. A similar trend is observed for FLAH$^\bullet$, with a potential of -1.16 V for 7,8-dimethyl-isoalloxazine and -1.22 V for lumiflavin and riboflavin, close to the -1.07 V of isoalloxazine. The difference in the redox potentials due to substitutions can be explained by the fact that electron donating groups like the methyl groups stabilize slightly the radical species via inductive effect. [80] Photoredox potentials in the excited state are on average 0.20 V lower compared to isoalloxazine, both for the singlet and triplet references. Overall, we observe the same trend that they become strong oxidizing agents in the excited state as isoalloxazine.

The acidity constants (pK$_a$) are affected by the redox state of flavin. Nitrogen centers N_1, N_3 and N_5 can undergo acid-base reactions. The computed pK$_a$ values of the FLA and its reduced forms in the ground state are shown in Table 2, including the pK$_a$ values for the usual N_5 acid-base reaction of FLA$^{\bullet-}$, and N_1 acid-base reaction for FLAH$^-$ for isoalloxazine, 7,8-dimethylisoalloxazine, lumiflavin and riboflavin. In addition, N_1 protonation of FLA$^{\bullet-}$ to lead to FLAH'$^\bullet$ and N_5 protonation of FLAH'$^-$ to lead to FLAH$_2$ (for isoalloxazine only) are also shown.

The lower pK$_a$ value for the FLA$^{\bullet-}$ than the FLAH$^-$ indicates higher proton affinity of the earlier which is likely because the proton affinity of the species decreases once it is already protonated in one site.

The calculated isoalloxazine pK$_a$ values are 10.6 for FLA$^{\bullet-}$ and 10.5 for FLAH$^-$ indicates that these are weak acids. A similar trend is observed for all the substituted forms.The calculated lumiflavin pK$_a$ values are 12.6 for FLA$^{\bullet-}$ and 10.7 for FLAH$^-$ indicates that these are weak acids. The experimental pK$_a$ value of FLA$^{\bullet-}$ and FLAH$^-$ in lumiflavin are 8.2 and 6.2 respectively, [82] therefore being stronger acids from what theoretical calculations predict. Still, the calculated values are in qualitative agreement with the experiments, that is, they reproduce the fact that FLAH$^-$ is a stronger acid than FLA$^{\bullet-}$ in the usual accuracy to which theory reproduce acidity constants. [59] pK$_a$ values are very difficult to reproduce quantitatively in calculations since they relate with the free energy with an exponential scale. Therefore, a small difference in energy can change the pKa value by a large value. More precisely, a 0.06 eV difference in energy can change the pKa value by one unit. Therefore, while comparing the experimental pKa with the theoretical one, normally the qualitative trend is compared instead of quantitative values. In case of riboflavin, the calculated values could not reproduce the right trend of the experimental pKa values. [83, 17] It should be noted that a quantitative reproduction of pKa values from theoretical calculation possibly requires to take explicit solvent effects into account, which is beyond the scope of the present manuscript. [59, 84]

The pK$_a$ values for the alternative protonation reaction, where N_1 is protonated first, show significantly less proton affinity (pK$_a$=5.6). Therefore, FLAH'$^\bullet$ is much more acidic than FLAH$^\bullet$. Thus, FLAH'$^\bullet$ can only be formed when N_5 position is blocked by a protecting group. Once the N_1 position is protonated, the proton affinity of the FLAH'$^-$ increases drastically for the protonation of N_5.

Table 2: Comparison of the (photo)reduction potentials E^0 for reduction processes and acidity constants (pK_a) of isoalloxazine and derivatives in ethanol. The calculated values of this work (calc) were performed using def2-TZVPP basis set and B3LYP functional, and matched to literature values (lit). FLAH'$^\bullet$ and FLAH$^\bullet$ correspond to the protonation to N_1 and N_5 positions, respectively with reference to ferrocene electrode (absolute reduction potential = 4.89 V). $^{1(3)}$FLA* refers to the singlet (triplet) photo-excited state of fully oxidized flavin, and FLAH and FLAH' correspond to the protonation to N_5 and N_1 positions, respectively. E^0 values are in Volts (V).

System	Process	E^0_{calc}	E^0_{lit}	Process	pK_a^{calc}	pK_a^{lit}
Isoalloxazine	FLA→FLA$^{\bullet-}$	-1.16	-1.21[a]	FLA$^{\bullet-}$ →FLAH$^\bullet$	10.6	
	^{1}FLA*→FLA$^{\bullet-}$	1.57		FLA$^{\bullet-}$ →FLAH'$^\bullet$	5.6	
	^{3}FLA*→FLA$^{\bullet-}$	0.80				
	FLAH$^\bullet$ → FLAH$^-$	-1.07				
	FLAH$^{\bullet*}$ → FLAH$^-$	1.1		FLAH$^-$ → FLAH$_2$	10.5	
	FLAH'$^\bullet$ → FLAH'$^-$	-1.79		FLAH'$^-$ → FLAH$_2$	27.2	
	FLAH'$^{\bullet*}$ → FLAH'$^-$	0.03				
7,8-dimethylisoalloxazine	FLA→FLA$^{\bullet-}$	-1.29		FLA$^{\bullet-}$ →FLAH$^\bullet$	11.6	
	^{1}FLA*→FLA$^{\bullet-}$	1.38				
	^{3}FLA*→FLA$^{\bullet-}$	0.52				
	FLAH$^\bullet$ → FLAH$^-$	-1.16		FLAH$^-$ → FLAH$_2$	10.6	
	FLAH$^{\bullet*}$ → FLAH$^-$	0.78				
Lumiflavin	FLA→FLA$^{\bullet-}$	-1.35		FLA$^{\bullet-}$ →FLAH$^\bullet$	12.6	8.2[b]
	^{1}FLA*→FLA$^{\bullet-}$	1.32				
	^{3}FLA*→FLA$^{\bullet-}$	0.48				
	FLAH$^\bullet$ → FLAH$^-$	-1.22		FLAH$^-$ → FLAH$_2$	10.7	6.2[b]
	FLAH$^{\bullet*}$ → FLAH$^-$	0.67				
Riboflavin	FLA→FLA$^{\bullet-}$	-1.33	$-1.25^{[c]}$(R) $-1.17^{[c]}$(O)	FLA$^{\bullet-}$ →FLAH$^\bullet$	12.7	8.37[e]
	^{1}FLA*→FLA$^{\bullet-}$	1.34				
	^{3}FLA*→FLA$^{\bullet-}$	0.49				
	FLAH$^\bullet$ → FLAH$^-$	-1.22	$-1.05^{[d]}$ $-0.95^{[c]}$	FLAH$^-$ → FLAH$_2$	13.02	6.7[e]
	FLAH$^{\bullet*}$ → FLAH$^-$	0.65				

Previous calculated and experimental values are taken from [a] Cyclic voltametry of 10-isopropyl-isoalloxazine obtained in Ref. 82. [b]Experimental pK_a values taken from Ref. 74 and references therein. [c] DFT calculations (PBE/DNP) and fluorescence spectro-electrochemical analysis of Ref. 58, [d] cyclic Voltametry 75 analysis. R stands for reduction and O for oxidation. [e]Experimental pK_a values are taken from Refs. 17, 83.
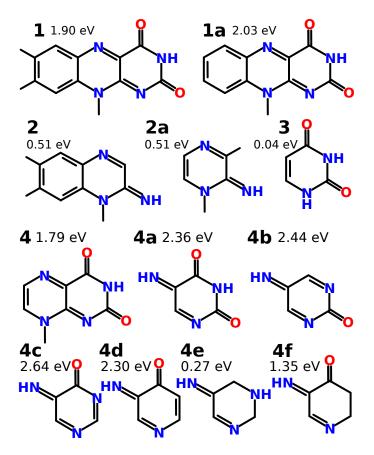
Figure 5: Structures for which we compute the electron affinities. Structure **1** corresponds to lumiflavin, **1a** is 10-methylisoalloxazine, and **3** is uracil. The other compounds are either cuts of these three rings and elimination or substitutions of heteroatoms.

3.3. Origin of the electron affinity of lumiflavin

The α-diimine bond is reduced to an ethene-1,2-diamine bond upon accepting 2 electrons and 2 protons. It is widely accepted that α-diimine bonds are good electron acceptors. These diimines are frequently used as non-innocent ligands in organometallic systems (where they are frequently referred as 1,4-diaza-1,3-dienes, DADs) and electron acceptors in donor-acceptor systems. [85, 86] However, it was recently discussed by Patel et al. that the diimine group is not enough to explain a strong electron affinity, showing that substituents can decrease the electron acceptor capacity or even make a diimine bond a bad electron acceptor. Here, we determine the origin of the electron acceptor capacity of isoalloxazine, and the role of the three rings in explaining its strong electron affinity. For this purpose, we cut the lumiflavin ring in constituent rings, which in[600] addition we modify by eliminating heteroatoms or substituting them with carbon centers. The resulting structures are shown in Figure 5.

We have computed first electron affinities (EA) and the molecular orbital at the origin of this EA. For lumiflavin, the EA is 1.903 eV, while isoalloxazine has an EA of 2.03 eV. The value of lumiflavin is in very good correspondence with the experimental value of lumiflavin 1.86 eV. [68] This

implies a good electron attractor for both lumiflavin and isoalloxazine. The methyl group of the o-xylene ring decrease the electron acceptor capacity of isoalloxazine by 0.127 eV. In order to determine the role of the constituent rings, we eliminated first one of the three rings, either the uracil-like ring (although keeping the α-diimine bond, compound **2**) or the o-xylene (compound **4**). The EA of **2** is 0.505 eV, while the EA of **4** is 1.793 eV, thus close to the lumiflavin EA. This shows that an α-diimine bond is not enough for explaining a strong electron acceptor property of flavins. Indeed, the uracil-like ring plays a direct role in making isoalloxazine a good electron acceptor. This implies that the heteroatoms present in the uracil-like ring ensure a high electron affinity. This observation is further confirmed when we compute the EA of the central ring alone (**2a**, 0.137 eV), in contrast with the uracil-like ring in which we keep the α-diimine bond (**4a**, 2.364 eV). Clearly, the α-diimine bond is the electron acceptor, since the uracil ring (**3**) has an electron affinity of 0.036 eV. This value compares very well with the experimental findings, which reported a value of 0.06 ± 0.03 eV electron affinity for uracil. [87]

In order to determine the role of heteroatoms in influencing electron affinity of isoalloxazine, we have performed several variations of compound **4** and **4a** by either substituting or eliminating heteroatoms in the uracil-like ring (**4-4f**). The **4** has an EA of 1.794 eV, similar to that of isoalloxazine. This implies that the o-xylene group has only a minor effect on the EA of isoalloxazine. The **4a** ring, which corresponds to an uracil-like ring with a diimine bond has 2.364 eV. This is similar to the **4b** (2.437 eV), **4c** (2.639 eV) and **4d** (2.295 eV), showing a strong electron affinity. All these structure have in common that they have strong electronegative oxygen atom and they are planar. In contrast, **4e** has an electron affinity of 0.271 eV. In this case, the structure is not planar and no carbonyl groups are present, leading to an electron affinity comparable to **2a** and **2**. Finally, the structure **4f**, which has an carbonyl group but it is not planar, has an EA of 1.355 eV.

In summary, we can attribute a strong electron affinity basically to the presence of an α-diimine bond and two more conditions: (i) a planar ring to stabilize the central double bond formed between the carbon atoms of the diimine bond, and (ii) the presence of electronegative oxygen atoms that stabilizes the π orbitals and decreases the interaction with delocalized Rydberg orbitals. The presence of electronegative groups seems to be the more important factor to increase the electron affinity. This is seen for example in **4f**, which has a carbonyl group but is not planar, resulting in an EA of 1.355 eV. On the other hand, **2** and **2a** are planar, but without strong electronegative groups, resulting also in a positive EA of 0.505 and 0.127 eV respectively. When both the planarity and the electronegative atoms are present (**4**, **4a**, **4b**, **4c** and **4d**), a strong negative electron affinity are observed.

4. Conclusions

The present work provides the first systematic theoretical study of the redox states of isoalloxazine in solution. We have performed a simulation of the main photophysical properties: UV-visible spectroscopy, redox potentials, acidity constants and electron affinities. In addition, we have critically evaluated the effect of substitutions on the main photophysical properties, by comparing isoalloxazine to 7,8-dimethylisoalloxazine, lumiflavin and riboflavin.

We show that the π_3 is the main orbital that explains the photophysics of isoalloxazine. This is a π^*-type orbital for the $N_5=C_{4a}$ and $C_{10a}=N_1$ double bonds and a π orbital for the C_{4a}-C_{10a}. Thus, upon reduction, the isoalloxazine α-diimine bond formed by the atoms $N_5=C_{4a}$-$C_{10a}=N_1$, which becomes an ethene-1,2-diamine HN_5-$C_{4a}=C_{10a}$-N_1H when it is fully reduced. This type of bond is frequently found in non-innocent ligands used in organometallic chemistry that can undergo a redox reaction by accepting electrons from the metal. They are also used in donor acceptor systems.

The π_3 bond is the lowest unoccupied orbital for oxidized form of FLA, a singly occupied orbital for the semiquinonic forms and the highest occupied orbital for the reduced forms. For the oxidized form and the semi-quinone forms, the $\pi_2 \to \pi_3$ transition is the transition with strongest oscillator strength. In the case of FLA and $FLA^{\bullet-}$, this transition is in the blue light region, while this transition is a broad band in the green-red light region for $FLAH^{\bullet}$. For $FLAH^-$ and $FLAH_2$, this transition is forbidden due to the two electrons occupying π_3. Therefore, the only possible transition for these two forms is the $\pi_3 \to \pi_4$ which is much higher in energy, in the UV light region.

We have computed redox (photo)redox potentials and acidity constants of isoalloxazine. For the reduction reactions of FLA and $FLAH^{\bullet}$, we find that they are weak oxidizing agents in their ground states, but become strong oxidizers in the excited state. In the case of FLA, the triplet state photoredox potential is weaker than the singlet state. The methylation of C_7 and C_8 decreases the redox potentials by -0.1 to -0.2 V on average with respect to isoalloxazine. However, the same trends are observed as for the core chromophore. The reduced anionic forms are acidic. We have confirmed that the N_5 center becomes more acidic that N_1 upon the first reduction, due to the electron distribution that debilitates the $N_5=C_{4a}$ double bond. In the second reduction step, the N_1 centre also becomes a strong acidic center.

Finally, we have computed the electron affinities of isoalloxazine and lumiflavin, showing a good comparison with experimental electron affinities. In order to determine the origin of the electron affinity of lumiflavin, we have performed a computation of electron affinities of smaller parts forming the isoalloxazine ring. We show that the α-diimine is fundamental to explain the electron affinity of isoalloxazine. The o-xylene ring in addition to the α-diimine does not show a strong electron affinity, whereas the α-diimine with the uracil-like ring has a similar electron affinity than isoalloxazine. We rationalize that both the planarity of the uracil rings and the electronegative oxygen atoms are essential to localize the π orbitals and avoid the mixture with Rydberg states, the latter factor being the most important one.

To conclude, we have determined the main photophysical properties of isoalloxazine chromophore, which are directly related to the existence of the α-diimine bond. The present study can help in designing more efficient electron acceptor molecules based on diimine motifs and non-innocent 1,4-diaza-1,3-dienes ligands.

References

[1] D. J. O'Kane, D. C. Prasher, Evolutionary origins of bacterial bioluminescence, Mol. Microbiol. 6 (1992) 443–449.

[2] F. Müller (Ed.), Chemistry and Biochemistry of Flavoenzymes, vols. i-iii Edition, CRC Press, Boca Raton, FL, 1990-1991.

[3] V. Massey, The chemical and biological versatility of riboflavin, Biochem. Soc. Trans. 28 (2000) 283–296.

[4] A. Sancar, Structure and function of DNA photolyase and cryptochrome blue-light photoreceptors, Chem. Rev. 103 (2003) 2203–2237.

[5] Y.-T. Kao, C. Saxena, L. Wang, A. Sancar, D. Zhong, Direct observation of thymine dimer repair in DNA by photolyase, Proc. Natl. Acad. Sci. 102 (2005) 16128–16132.

[6] I. A. Solov'yov, D. Chandler, K. Schulten, Magnetic field effects in arabidopsis thaliana cryptochrome-1, BioPhys. J 92 (2007) 2711–2726.

[7] I. A. Solov'yov, H. Mouritsen, K. Schulten, Acuity of a cryptochrome and vision based magnetoreception system in birds, BioPhys. J 99 (2010) 40–49.

[8] M. Medina, R. Cammack, Flavoproteins involved in photosynthetic electron transport in the cyanobacterium anabaena sp pcc 7119. electron spin-echo envelope modulation spectroscopic studies, J. Chem. Soc., Perkin Trans. 2 0 (1996) 633–638.

[9] S. A. Susin, H. K. Lorenzo, N. Zamzami, I. Marzo, B. E. Snow, G. M. Brothers, J. Mangion, E. jacotot, P. Constantini, M. Loeffler, N. Larochette, D. R. Goodlett, R. Aebersold, D. P. Siderovski, J. M. Penninger, G. Kroemer, Molecular characterization of mitochondrial apoptosis-inducing factor, Nature 397 (1999) 441–446.

[10] Y. C. Chen, S. Y. Lin-Shiau, J. K. Lin, Involvement of reactive oxygen species and caspase 3 activation in arsenite-induced apoptosis, J. Cell. Physiol. 177 (1998) 324–333.

[11] S. Dagley, Lessons from biodegradation, Annu. Rev. Microbiol. 41 (1987) 1–23.

[12] H. Z. Chen, S. L. Hopper, C. E. Cerniglia, Biochemical and molecular characterization of an azoreductase from staphylococcus aureus, a tetrameric NADPH-dependent flavoprotein, Microbiol. 151 (2005) 1433–1441.

[13] M. Gomelsky, G. Klug, BLUF: a novel FAD-binding domain involved in sensory transduction in microorganisms, Trends Biochem. Sci. 27 (2002) 497–500.

[14] S. L. DeBlasio, D. L. Luesse, R. P. Hangarter, A plant-specific protein essential for blue-light-induced chloroplast movements, Plant Physiol. 139 (2005) 101–114.

[15] E. Silva, A. M. Edwards, D. Pacheco, Visible light-induced photooxidation of glucose sensitized by riboflavin, J. Nut. Biochem. 10 (1999) 181–185.

[16] L. de O. R. Arrivetti, R. S. Scurachio, W. G. Santos, T. B. R. Papa, L. H. Skibsted, D. R. Cardoso, Photooxidation of other B-vitamins as sensitized by riboflavin, J. Agric. Food Chem. 61 (2013) 7615–7620.

[17] Y.-T. Kao, C. Saxena, T.-F. He, L. Guo, L. Wang, A. Sancar, D. Zhong, Ultrafast dynamics of flavins in five redox states, J. Am. Chem. Soc. 130 (2008) 13132–13139.

[18] J. Koziol, Absorption spectra of riboflavin, lumiflavin, and lumichrome in organic solvents, Experientia 21 (1965) 189–190.

[19] J. Koziol, Studies on flavins in organic solvents – I. spectral characteristics of riboflavin, riboflavin tetrabutyrate and lumichrome, Photochem. Photobiol 5 (1966) 41–54.

[20] J. Koziol, Studies on flavins in organic solvents – iii. spectral behaviour of lumiflavin, Photochem. Photobiol 9 (1969) 45–53.

[21] A. Weigel, A. L. Dobryakov, M. Veiga, J. L. P. Lustres, Photoinduced processes in riboflavin: Superposition of $\pi\pi^*$–$n\pi^*$ states by vibronic coupling, transfer of vibrational coherence, and population dynamics under solvent control, J. Phys. Chem. A 112 (2008) 12054–12065.

[22] P. Zirak, A. Penzkofer, T. Mathes, P. Hegemann, Photodynamics of roseoflavin and riboflavin in aqueous and organic solvents, Chem. Phys. 358 (2009) 111–122.

[23] T. Kottke, J. Heberle, D. Hehn, B. Dick, P. Hegemann, Phot-LOV1: photocycle of a blue-light receptor domain from the green alga chlamydomonas reinhardtii, Biophys. J. 84 (2003) 1192–1201.

[24] E. Sikorska, I. V. Khmelinskii, J. Koput, J. L. Bourdelande, M. Sikorski, Electronic structure of isoalloxazines in their ground and excited states, J. Molec. Struct. 697 (2004) 137–141.

[25] A. Penzkofer, Absorption and emission spectroscopic investigation of alloxazine in aqueous solutions and comparison with lumichrome, J. Photochem. Photobiol. A: Chem 314 (2016) 114–124.

[26] C. B. Martin, X. Shi, M.-L. Tsao, D. Karweik, J. Brooke, C. M. Hadad, M. S. Platz, The photochemistry of riboflavin tetraacetate and nucleosides. a study using density functional theory, laser flash photolysis, fluorescence, UV–vis, and time resolved infrared spectroscopy, J. Phys. Chem. B 106 (2002) 10263–10271.

[27] M. Takahashi, Y. Ishikawa, J.-i. Nishizawa, H. Ito, Low-frequency vibrational modes of riboflavin and related compounds, Chem. Phys. Lett. 401 (2005) 475–482.

[28] S. Salzmann, J. Tatchen, C. M. Marian, The photophysics of flavins: What makes the difference between gas phase and aqueous solution?, J. Photochem. Photobiol. A: Chem. 198 (2008) 221–231.

[29] S. Salzmann, C. M. Marian, Effects of protonation and deprotonation on the excitation energies of lumiflavin, Chem. Phys. Lett. 463 (2008) 400–404.

[30] J.-y. Hasegawa, S. Bureekaew, H. Nakatsuji, Sac-ci theoretical study on the excited states of lumiflavin: Structure, excitation spectrum, and solvation effect, J. Photochem. Photobiol. A: Chem. 189 (2007) 205–210.

[31] M. M. N. Wolf, C. Schumann, R. Gross, T. Domratcheva, R. Diller, Ultrafast infrared spectroscopy of riboflavin: Dynamics, electronic structure, and vibrational mode analysis, J. Phys. Chem. B 112 (2008) 13424–13432.

[32] C. Neiss, P. Saalfrank, M. Parac, S. Grimme, Quantum chemical calculation of excited states of flavin-related molecules, J. Phys. Chem. A 107 (2003) 140–147.

[33] M. Dittric, P. L. Freddolino, K. Schulten, Dynamic switching mechanisms in LOV1 and LOV2 domains of plant phototropins., J. Phys. Chem. B 109 (2005) 13006–13013.

[34] B. Klaumünzer, D. Kröner, P. Saalfrank, (td-)dft calculation of vibrational and vibronic spectra of riboflavin in solution, J. Phys. Chem. B 114 (2010) 10826–10834.

[35] Y.-K. Choe, S. Nagase, K. Nishimoto, Theoretical study of the electronic spectra of oxidized and reduced states of lumiflavin and its derivative, J. Comput. Chem. 28 (2007) 727–739.

[36] B. Liu, H. Liu, D. Zhong, C. Lin, Searching for a photocycle of the cryptochrome photoreceptors, Curr. Opin. Plant Biol. 13 (2010) 578–586.

[37] S. Ren, M. Sawada, K. Hasegawa, Y. Hayakawa, H. Ohta, S. Masuda, A PixDPapB chimeric protein reveals the function of the BLUF domain C-terminal α-helices for light signal transduction, Plant Cell Physiol. 53 (2012) 1638–1647.

[38] C. Nielsen, M. S. Norby, J. Kongsted, I. A. Solov'yov, Absorption spectra of FAD embedded in cryptochromes, J. Phys. Chem. Lett. 9 (2018) 3618–3623.

[39] T. Climent, R. Gonzalez-Luque, M. Merchand, L. Serrano-Andres, Theoretical insight into the spectroscopy and photochemistry of isoalloxazine, the flavin core ring, J. Phys. Chem. A 110 (2006) 13584–13590.

[40] M. Wu, L. A. Eriksson, Absorption spectra of riboflavina difficult case for computational chemistry, J. Phys. Chem. A 114 (2010) 10234–10242.

[41] E. Sikorska, I. V. Khmelinskii, W. Prukala, S. L. Williams, M. Patel, D. R. Worrall, J. L. Bourdelande, J. Koput, M. Sikorski, Spectroscopy and photophysics of lumiflavins and lumichromes, J. Phys. Chem. A 108 (2004) 1501–1508.

[42] I. A. Solovyov, T. Domratcheva, A. R. Moughal Shahi, K. Schulten, Decrypting cryptochrome: Revealing the molecular identity of the photoactivation reaction, J. Am. Chem. Soc. 134 (43) (2012) 18046–18052.

[43] R. K. Kar, V. A. Borin, Y. Ding, J. Matysik, I. Schapiro, Spectroscopic properties of lumiflavin: A quantum chemical study, Photochem. Photobiol. 95 (2019) 662–674.

[44] L. Zanetti-Polzi, M. Aschi, I. Daidone, A. Amadei, Theoretical modeling of the absorption spectrum of aqueous riboflavin, Chem. Phys. Lett. 669 (2017) 119 – 124.

[45] B. Karasulu, J. P. Götze, W. Thiel, Assessment of FranckCondon methods for computing vibrationally broadened UVvis absorption spectra of flavin derivatives: Riboflavin, roseoflavin, and 5-thioflavin, J. Chem. Theor. Comput. 10 (2014) 5549–5566.

[46] C. Nielsen, M. S. Nørby, J. Kongsted, I. A. Solov'yov, Absorption spectra of fad embedded in cryptochromes, J. Phys. Chem. Lett. 9 (2018) 3618–3623.

[47] A. Mukherjee, C. M. Schroeder, Flavin-based fluorescent proteins: emerging paradigms in biological imaging, Curr. Opin. Biotech. 31 (2015) 16–23.

[48] S. Salzmann, V. Martinez-Junza, B. Zorn, S. E. Braslavsky, M. Mansurova, C. M. Marian, W. Grtner, Photophysical properties of structurally and electronically modified flavin derivatives determined by spectroscopy and theoretical calculations, J. Phys. Chem. A 113 (2009) 9365–9375.

[49] C. Hou, Y.-J. Liu, N. Ferré, W.-H. Fang, Understanding bacterial bioluminescence: A theoretical study of the entire process, from reduced flavin to light emission, Chem. Eur. J. 20 (2014) 7979–7986.

[50] M. G. Khrenova, A. V. Nemukhin, T. Domratcheva, Theoretical characterization of the flavin-based fluorescent protein iLOV and its Q489K mutant, J. Phys. Chem. B 119 (2015) 5176–5183.

[51] A. Tyagi, A. Penzkofer, pH dependence of the absorption and emission behaviour of lumiflavin in aqueous solution, J. Photochem. Photobiol. A: Chem. 215 (2010) 108–117.

[52] A. Baiardi, J. Bloino, V. Barone, General time dependent approach to vibronic spectroscopy including Franck-Condon, Herzberg-Teller, and Duschinsky effects, J. Chem. Theor. Comput. 9 (2013) 4097–4115.

[53] A. D. Becke, Densityfunctional thermochemistry. iii. the role of exact exchange, J. Chem. Phys. 98 (1993) 5648–5652.

[54] C. Lee, W. Yang, R. G. Parr, Development of the colle-salvetti correlation-energy formula into a functional of the electron density, Phys. Rev. B 37 (1988) 785–789.

11

[55] J. Tomasi, B. Mennucci, R. Cammi, Quantum mechanical continuum solvation models, Chem. Rev. 105 (2005) 2999–3094.

[56] G. Scalmani, M. J. Frisch, Continuous surface charge polarizable continuum models of solvation. i. general formalism, J. Chem. Phys. 132 (2010) 114110–114115.

[57] J. Bloino, M. Biczysko, F. Santoro, V. Barone, General approach to compute vibrationally resolved one-photon electronic spectra, J. Chem. Theor. Comput. 6 (2010) 1256–1274.

[58] W. Chen, J.-J. Chen, R. Lu, C. Qian, W.-W. Li, H.-Q. Yu, Redox reaction characteristics of riboflavin : A fluorescence spectroelectrochemical analysis and density functional theory calculation, Bioelectrochemistry 98 (2014) 103–108.

[59] K. S. Alongi, G. C. Schields, Theoretical calculations of acid dissociation constants: A review article, Ann. Rep. Comput. Chem. 6 (2010) 113–138.

[60] C. P. Kelly, C. J. Cramer, D. G. Truhlar, Aqueous solvation free energies of ions and ion-water clusters based on an accurate value for the absolute aqueous solvation free energy of the proton, J. Phys. Chem. B 110 (2006) 16066–16081.

[61] M. J. Frisch, G. W. Trucks, H. B. Schlegel, G. E. Scuseria, M. A. Robb, J. R. Cheeseman, G. Scalmani, V. Barone, G. A. Petersson, H. Nakatsuji, X. Li, M. Caricato, A. V. Marenich, J. Bloino, B. G. Janesko, R. Gomperts, B. Mennucci, H. P. Hratchian, J. V. Ortiz, A. F. Izmaylov, J. L. Sonnenberg, D. Williams-Young, F. Ding, F. Lipparini, F. Egidi, J. Goings, B. Peng, A. Petrone, T. Henderson, D. Ranasinghe, V. G. Zakrzewski, J. Gao, N. Rega, G. Zheng, W. Liang, M. Hada, M. Ehara, K. Toyota, R. Fukuda, J. Hasegawa, M. Ishida, T. Nakajima, Y. Honda, O. Kitao, H. Nakai, T. Vreven, K. Throssell, J. A. Montgomery, Jr., J. E. Peralta, F. Ogliaro, M. J. Bearpark, J. J. Heyd, E. N. Brothers, K. N. Kudin, V. N. Staroverov, T. A. Keith, R. Kobayashi, J. Normand, K. Raghavachari, A. P. Rendell, J. C. Burant, S. S. Iyengar, J. Tomasi, M. Cossi, J. M. Millam, M. Klene, C. Adamo, R. Cammi, J. W. Ochterski, R. L. Martin, K. Morokuma, O. Farkas, J. B. Foresman, D. J. Fox, Gaussian 16 Revision A.01, gaussian Inc. Wallingford CT (2016).

[62] M. Sakai, H. Takahashi, One-electron photoreduction of flavin mononucleotide: time-resolved resonance Raman and absorption study, J. Molec. Struct. 379 (1996) 9–18.

[63] S. Ghisla, V. Massey, J.-M. Lhoste, S. G. Mayhew, Fluorescence and optical characteristics of reduced flavines and flavoproteines, Biochem. 13 (1974) 589–597.

[64] C.-W. Chang, T.-F. He, L. Guo, J. A. Stevens, T. Li, L. Wang, D. Zhong, Mapping solvation dynamics at the function site of flavodoxin in three redox states, J. Am. Chem. Soc. 132 (2010) 12741–12747.

[65] A. Lukacs, R.-K. Zhao, A. Haigney, R. Brust, G. M. Greetham, M. Towrie, P. J. Tonge, S. R. Meech, Excited state structure and dynamics of the neutral and anionic flavin radical revealed by ultrafast transient mid-ir to visible spectroscopy, J. Phys. Chem. B 116 (2012) 5810–5818.

[66] F. Muller, M. Brustlein, P. Hemmerich, V. Massey, W. H. Walker, Light-absorption studies on neutral flavin radicals, Eur. J. Biochem. 25 (1972) 573–580.

[67] P. Kamaev, M. Smirnov, M. Friedman, D. Muller, Aggregation and photoreduction in anaerobic solutions of flavin mononucleotide,, J. Photochem. Photobiol. A: Chem. 310 (2015) 60–65.

[68] T. Zhang, K. Papson, R. Ochran, D. P. Ridge, Stability of flavin semiquinones in the gas phase: The electron affinity, proton affinity, and hydrogen atom affinity of lumiflavin, J. Phys. Chem. A 117 (2013) 11136–11141.

[69] R.-K. Zhao, A. Lukacs, A. Haigney, R. Brust, G. M. Greetham, M. Towrie, P. J. Tonge, S. R. Meech, Ultrafast transient mid ir to visible spectroscopy of fully reduced flavins, Phys. Chem. Chem. Phys. 13 (2011) 17642–17648.

[70] V. A. Crawford, 420. Hyperconjugation. Part III. Bathochromic shifts resulting from methyl substitution in conjugated systems, J. Chem. Soc. (1953) 2061–2065.

[71] S. V. Tatwawadi, K. S. V. Santhanam, A. J. Bard, The electrochemical reduction of riboflavin in dimethylsulfonoxide, J.

[72] J. J. Hasford, C. J. Rizzo, Linear free energy substituent effect on flavin redox chemistry, J. Am. Chem. Soc. 120 (1998) 2251–2255.

[73] J. D. Walsh, A.-F. Miller, Flavin reduction potential tuning by substitution and bending, J. Molec. Struct. (Theochem) 623 (2002) 185–195.

[74] C. Bonazzola, G. Gordillo, Electrochemistry of lumiflavin adsorbed at mercury acidic aqueous solution interface, J. Electroanal. Chem. 599 (2007) 356–366.

[75] S. L. J. Tan, R. D. Webster, Electrochemically indiced chemically reversible proton-coupled electron transfer reactions of riboflavin (vitamin b_2), J. Am. Chem. Soc. 134 (2012) 5954–5964.

[76] K. Arumugam, U. Becker, Computational redox potential predictions: Application to inorganic and organic aqueous complexes, and complexes adsorbed to mineral surfaces., minerals 4 (2014) 345–387.

[77] A. M. Edwards, Structure and general properties of flavins, in: S. Weber, E. Schleicher (Eds.), Flavins and Flavoproteins: Methods and Protocols, Springer New York, 2014, Ch. 1, pp. 3–13.

[78] R. M. Kowalczyk, E. Schleicher, R. Bittl, S. Weber, The photoinduced triplet of flavins and its protonation states, J. Am. Chem. Soc 126 (2004) 11393–11399.

[79] D. E. Edmondson, S. Ghisla, Electronic effects of 7 and 8 ring substituents as predictors of flavin oxidation-reduction potentials, in: Flavins and flavoproteins 1999 : proceedings of the Thirteenth International Symposium, Konstanz, Germany, August 29 - September 4, 1999, 1999, pp. 71–76.

[80] D. E. Edmondson, R. De Francesco, Structure, synthesis, and physical properties of covalently bound flavins and 6- and 8-hydroxyflavins, in: F. Muller (Ed.), Chemistry and Biochemistry of Flavoenzymes, Taylor& Francis, 1999, Ch. 2, p. 31.

[81] A. Kormanyos, M. S. Hossain, G. Ghadimkhani, J. J. Johnson, C. Janky, N. R. de Tacconi, F. W. Foss Jr., Y. Paz, K. Rajeshwar, Flavin derivatives with tailored redox properties: Synthesis, characterization, and electrochemical behavior, Chem. Eur. J. 22 (2016) 9209–9217.

[82] Y.-M. Legrand, M. Gray, G. Cooke, V. M. Rotello, Model systems for flavoenzyme activity: relationships between cofactor structure, binding and redox properties, J. Am. Chem. Soc 125 (51) (2003) 15789–15795.

[83] F. Müller, The Flavin Redox-System and Its Biological Function. In Topics of Current Chemistry, F. L. Boschke (Ed.), 108th Edition, Springer-Verlag, Berlin, 1983.

[84] M. Kilic, B. Ensing, Acidity constants of lumiflavin from first principles molecular dynamics simulations, Phys. Chem. Chem. Phys. 16 (2014) 18993–19000.

[85] E. Uhlig, Non-innocent bidentate nitrogen-ligands in electron-rich complexes of 3d-elements, Pure and Applied Chemistry 60 (1988) 1235.

[86] D. G. D. Patel, F. Feng, Y.-y. Ohnishi, K. A. Abboud, S. Hirata, K. S. Schanze, J. R. Reynolds, It takes more than an imine: The role of the central atom on the electron-accepting ability of benzotriazole and benzothiadiazole oligomers, J. Am. Chem. Soc. 134 (2012) 2599–2612.

[87] C. Desfrancois, V. Periquet, Y. Bouteiller, J. P. Schermann, Valence and dipole binding of electrons to uracil, J. Chem. Phys. A 102 (1998) 1274–1278.

FLA   FLA$^{\bullet-}$ FLAH$^{\bullet}$ FLAH^{-} FLAH$_2$

Abs.:

Blue   Blue   Green   UV   UV

Emiss.:

Green   Green   Red   Green   Green